Optics Communications 359 (2016) 393–398

Contents lists available at ScienceDirect

Optics Communications

journal homepage: www.elsevier.com/locate/optcom

Spatial and spectral selective characteristics of the plasmonic sensing using metallic nanoslit arrays

Caiwang Ge [a], Zhongyi Guo [a,b,*], Yongxuan Sun [b], Fei Shen [b], Yifei Tao [b], Jingran Zhang [b], Rongzhen Li [b], Linbao Luo [a]

[a] School of Electronics Science and Applied Physics, Hefei University of Technology, Hefei 230009, China
[b] School of Computer and Information, Hefei University of Technology, Hefei 230009, China

ARTICLE INFO

Article history:
Received 17 July 2015
Received in revised form
30 September 2015
Accepted 1 October 2015

Keywords:
Biosensing
Nanoslit arrays
Cavity mode
Surface plasmon polaritons (SPPs)
Spatial and frequency selective

ABSTRACT

A novel spatial and spectral selective plasmonic sensing based on the metal nanoslit arrays has been proposed and investigated theoretically, which shows a high performance in the multiplexing biomolecular detections. By properly tuning the geometric parameters of metal nanoslit arrays, the enhanced optical fields at different regions can be obtained selectively due to the excitation of SPP, cavity mode (CM), and their coupling effects. Simulation results show that the resonances of the metal nanoslit arrays at different spatial locations and different wavelengths can be achieved simultaneously. A relative bigger red-shift of 57 nm can be realized when a layer of biomolecular film is adsorbing at the slit walls, and the corresponding total intensity difference will be enhanced near 10 times compared to that at the top surface. In addition, when a BSA protein monolayer is adsorbing at slit walls with different slit widths, the corresponding wavelength shifts can reach to more than 80 nm by modulating the widths of the slit. The simulated results demonstrate that our designed metal nanoslit arrays can serve as a portable, low-cost biosensing with a high spatial and spectral selective performance.

1. Introduction

Surface plasmon resonance (SPR) sensing, a label-free and real-time sensing, has attracted extensive interests due to their wide applications in medical diagnostics, drug discovery, environmental sensing, and food safety monitoring [1–4]. Currently, commercially available sensors are dominated by the conventional propagating surface plasmon resonance (PSPR)-based systems, such as utilizing noble metal films or prisms [5,6]. Although the commercial PSPR-based sensors provide relatively high sensitivity, these systems require some complex and expensive equipments to couple and monitor lights, which hinders it's pervasive applications because it is difficult to be integrated into portable and low-cost microfluidic sensing devices [7]. Recently, the characteristics based on the extraordinary optical transmission (EOT) of the nanostructures has been utilized for biosensing applications [8]. In particular, nanoplasmonic sensors based on EOT through periodic nanoaperture arrays in metallic films provide relatively high sensitivities [9,10]. The resonance mechanisms behind EOT have been proved theoretically and experimentally, which mainly correspond to the SPP and cavity mode (CM) [11–14]. There are many applications by using SPP [15–17] and CM [18–19], but here we consider to combine the SPP and CM for plasmonic sensing. The resonant spectra of the SPP and CM sensitively vary with the structure parameters and the refractive index environment around the sensor.

EOT-based sensors have been widely discussed in some literatures. And many researchers have developed and optimized some sensors with different strategies, such as using suspended metal films [20], changing the shape of nanoapertures [21], employing more complex structures [22], and so forth. However, in most previous studies on the EOT-based sensors, they focus on optimizing the far-field sensor for the bulk refractive index changes. Just a few researchers have exploited alternative opportunities to develop the sensing performances by utilizing the plasmonics effects in enhanced near-field. For example, a novel important feature of the sensing mechanism with spatially selective sensing has been exploited by properly tuning the geometric parameters of a gold nanoslit array to tailor the spatial distribution of the enhanced optical field [10]. It is believable that the sensor will be more sensitive to refractive index changes in the close vicinity of the metallic structure, because the detected molecules lies in the confined and enhanced optical field. In addition, besides the spatial selective sensing of plasmon systems, there is another way to further improve sensor′s performance by combining series of sensing unit cells with different resonant wavelengths for

* Corresponding author at: School of Electronics Science and Applied Physics, Hefei University of Technology, Hefei 230009, China.
E-mail addresses: guozhongyi@hfut.edu.cn (Z. Guo), luolb@hfut.edu.cn (L. Luo).

http://dx.doi.org/10.1016/j.optcom.2015.10.005
0030-4018/

multiplexing detection [23]. Recently, by properly tuning the geometric parameters of a multi-layered metallic cross-shaped antennas, spatially and spectral selective plasmonic sensing in a multispectral plasmon resonance system has been demonstrated in theory [24], which has a superior performance in plasmonic biosensing, detection and imaging. However, it is limited by the complicated process for the corresponding structural fabrication.

In this letter, we present a simple structure of metal nanoslit arrays, which can realize the spatial and spectral selective plasmonic sensing for the biomolecules. We have investigated the sensing responses of the moleculars adsorbing at metal top surface and inside the nanoslit. And the simulated results show that the responses of the plasmonics sensing exhibit a multiband characteristics in the visible and near-infrared regions due to the excitations of SPP, CM and their coupling effects. By properly tuning the geometric parameters of the nanoslit arrays, the better sensing regions can be spatially transformed between the nanoslit walls and the top surface. Meanwhile, there also exist a spectral selective response for the different geometric conditions. These results show a higher performance in spatial and spectral selective sensing. And the surprisingly large peak shift of 57 nm can be obtained for a 5-nm-thick biomolecular film with a refractive index of 1.570. This novel spatial and spectral selective plasmonic sensing offers a new opportunity to optimize the performance of EOT-based biosensors and has a potential application in multiplexing biomolecular detections.

2. Structure and simulation

As depicted in Fig. 1, we consider a periodic array of subwavelength metallic nanoslits deposited on the polymethyl methacrylate (PMMA) substrate (with the depth of $d=200$ nm) as the samples. The period, the width and depth of the slit are indicated as P, W and D, respectively. In the following simulations, we set the environmental material on the top metal surface and inside the region of the nanoslits to be the air or water. The simulations are carried out by finite element method (FEM) to analyze the optical responses of the selected simulating unit cell. The refractive index of PMMA is 1.5 here, and the permittivity of the used silver is obtained from reference [25]. We set the periodic boundary conditions in both of the x and y directions. And the perfectly matching layers (PMLs) are utilized at the calculated region boundaries to reduce the influence of light reflection. The transverse magnetic (TM) polarized light is incident normally from the top of the structure.

3. Results and discussions

3.1. Optical properties of the nanoslit arrays

In general, there will be the resonant modes in the transmitted spectra, such as the cavity modes (CM) and the SPP modes, existing in the metallic nanoslits with suitable parameters (including the depth of the film, the period and the width of the nanoslits). When the depth of the deposited metal film is large enough, there will exist multi-order cavity modes in the transmitted spectra, which can be marked as CMi respectively, and i denote the orders of the CM in the nanoslits, corresponding to the number of nodes in the magnetic field distributions [26]. Firstly, we consider a thinner nanoslit arrays with $D=50$ nm, $P=500$ nm, and $W=26$ nm, respectively. As shown in Fig. 2, there is just one transmission peak in the corresponding transmitted spectrum, which can be attributed to the excitation of the SPP on the PMMA/metal interface. And it can be confirmed in the Fig. 3(a), where the

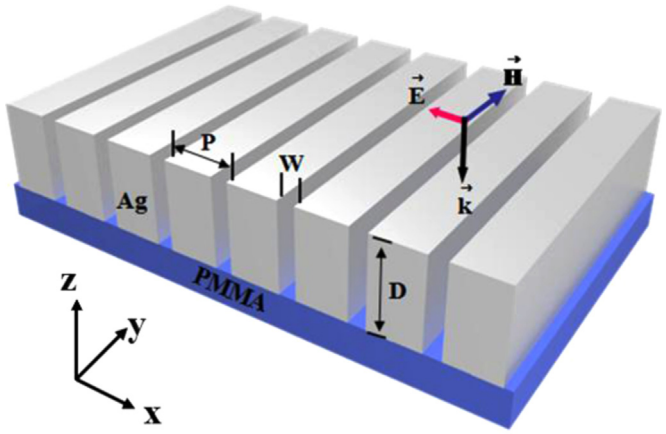

Fig. 1. Schematic of a metallic nanoslit arrays deposited on the PMMA, with the geometrical parameters (P, W and D), and the direction of the TM-polarized incident light.

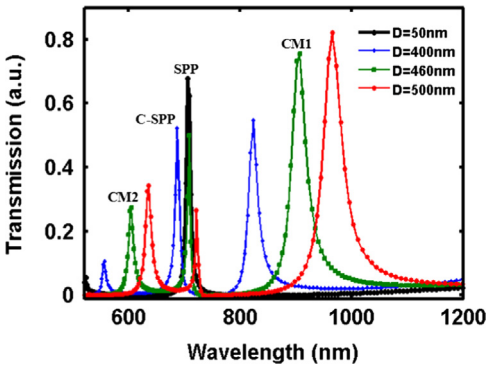

Fig. 2. Transmitted spectra of nanoslit arrays with different depths ($P=500$ nm, $W=26$ nm).

magnetic field (|Hy|) at the resonance wavelength (707 nm) can demonstrate the typical SPP characteristics near the PMMA/metal interface clearly.

For a normal incidence, λ_{spp} can be described by following equation [27]:

$$\lambda_{spp}(n, i) = \frac{P}{i} Re\left\{\left(\frac{\varepsilon_m n^2}{\varepsilon_m + n^2}\right)^{1/2}\right\} \quad (1)$$

where n is the refractive index of environmental materials, i denotes the resonant order, P is the period of the nanoslit arrays and ε_m is the dielectric constant of the metal. The equation shows the SPP's resonant wavelength is sensitive to the variation of the environmental refractive index, which can be used as SPP based sensors. When the depths of the metal nanoslit (D) are increased from 400 nm to 500 nm, as shown in Fig. 2, there will be three transmission peaks in every transmitted spectrum, which have been marked as the CM1, C-SPP, and CM2 respectively. The peaks of CM1 and CM2 are the first and second orders of the cavity modes in nanoslits. As shown in Fig. 3(b) and (d), for the nanoslit with the depths of $D=460$ nm, under the normal incidences of 605 nm and 907 nm light separately, the number of nodes in the magnetic field distributions are 1 and 2 respectively, which agree well with theoretical expectations. As depicted in Fig. 3(c), for the nanoslit with the depths of 460 nm, under the normal incidence of 709 nm light, there coexist the CM and the SPP mode in the magnetic field distributions. Therefore, the C-SPP peaks can be attributed as the couplings of CMs in nanoslits and the excited SPP on the metal surface. From Fig. 2, we can observe that for the

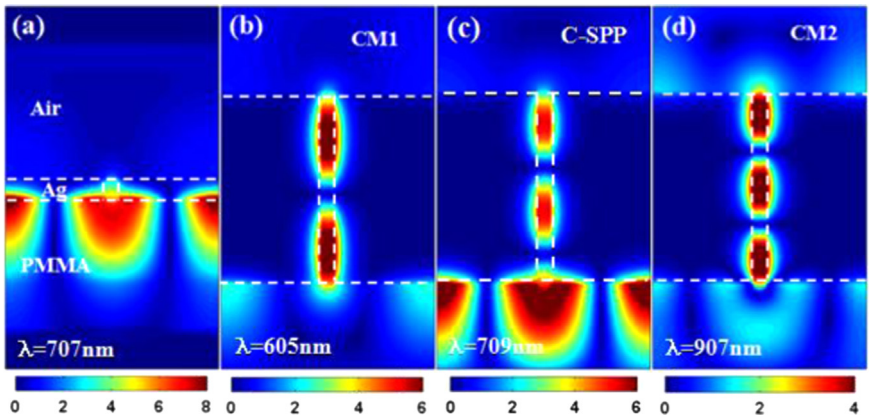

Fig. 3. Calculated magnetic field distributions at the corresponding resonances for the structures with $D=50$ nm (a), and $D=460$ at CM1 (b), C-SPP (c), CM2 (d). The white dotted lines mark the boundaries of the metallic films.

samples with $D=400$ nm, 460 nm and 500 nm, there exist CM1, CM2 and C-SPP peaks in the range of 450–1000 nm. Meanwhile, with increasing D, the transmission peaks of CMs have also a red-shift accordingly, and the peak intensity will increase too. It is worth noting that the C-SPP peaks will also shift to longer wavelength but with reducing intensity because the weaker coupling effect bewteen SPP and CMs.

In addition to the slit depth (D), the array period (P) and slit width (W) will also play important roles in nanoslit arrays' spectral responses. Fig. 4(a) shows the transmitted spectra of the nanoslit arrays by varying the periods (P) while the other parameters are kept the same ($D=460$ nm, $W=26$ nm). With increasing P, for the CM1 and CM2, the transmission spectrums have a small red shift and a decreasing transmission intensity. Nevertheless, there are an obvious red-shift for the C-SPP peaks because the array period directly impacts the SPP mode according to Eq. (1). Fig. 4 (b) shows the wavelength shifts of the three transmission peaks as a function of the nanoslit width (W) (with same $D=460$ nm and $P=500$ nm). Evidently, with increasing W, all peaks of the CM1, CM2 and C-SPP have a blue-shift accordingly, but the two CM curves are steeper than that of the C-SPP. It is easy to understand that small changes at slit width has a less effect on SPP mode (relating to the period directly), but with a direct effect on CM. Moreover, these wavelength-dependent peaks supply an available method to spectral selective sensing. Fig. 4(b) also indicated that our designed structure can offer a wideband (550–1200 nm) detection according to the concrete sensing requirements. In a word, the different resonance modes (SPP, CMi, C-SPP) with different characteristics, can offer a unique spatial and spectral selective sensing.

3.2. Spatial and spectral selective sensing

In order to investigate the sensing responses of the nanoslit arrays, the designed structure with the concrete parameters of $P=500$ nm, $D=460$ nm, $W=26$ nm, is placed in water environment with the refractive index of $n=1.33$. There are five obvious transmission peaks in the transmitted spectrum as shown in Fig. 5, which have been indicated as CM1 ($\lambda=1130$ nm), CM2 ($\lambda=798$ nm), CM3 ($\lambda=583$ nm), C-SPP1 ($\lambda=704$ nm), C-SPP2 ($\lambda=644$ nm), respectively. Fig. 6(a–c) show the calculated magnetic field distributions for the resonances in CM1, CM2 and CM3 at the corresponding incident wavelengths respectively. And we can observe the corresponding nodes' numbers in the magnetic field distributions are 1, 2 and 3 respectively. As depicted in Fig. 6 (d) and (e), we can know that the resonances in C-SPP1 and C-SPP2 are originating from the coupling between the CMs and SPP modes at PMMA/metal interface and water/metal interface respectively.

To validate the spatial tunability of the enhanced optical field and the associated spatially selective sensitivity, we have explored the sensor's responses on the molecules adsorbing at different positions of the structure. Here, we consider a 5 nm-thick dielectric film ($n=1.570$) adsorbing at the top surface of the metal arrays (Fig. 7(a)) or on the walls of the nanoslits (Fig. 7(b)). As shown in Fig. 7(c), for the case of the film adsorbing at the top surface, the resonance wavelengths' red shifts are 1.6 nm, 1.1 nm, 1.5 nm, 0.9 nm, 2.4 nm for CM1, CM2, CM3, C-SPP1 and C-SPP2

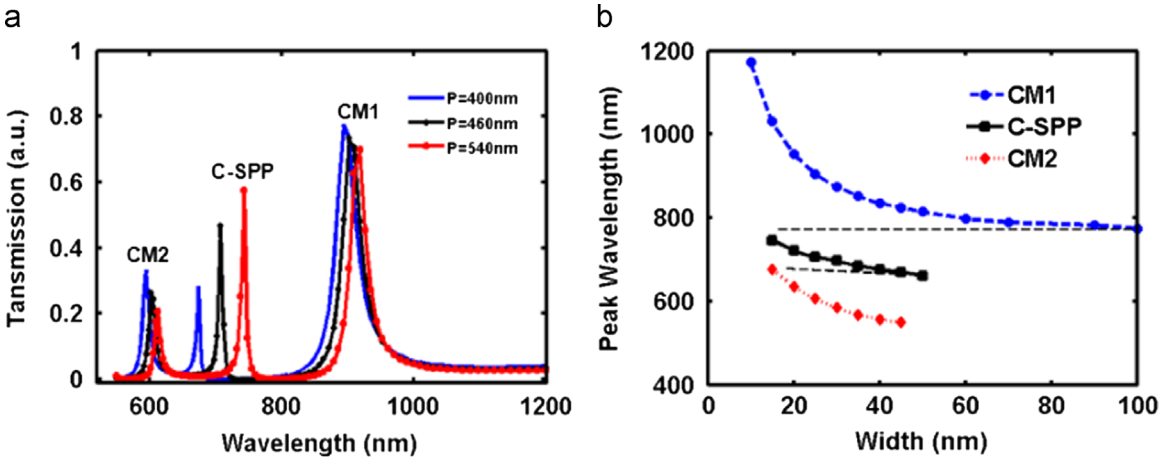

Fig. 4. Transmitted spectra of the proposed structures for different periods of nanoslit arrays (a), and the peaks positions (wavelength) as the functions of nanoslit widths (b).

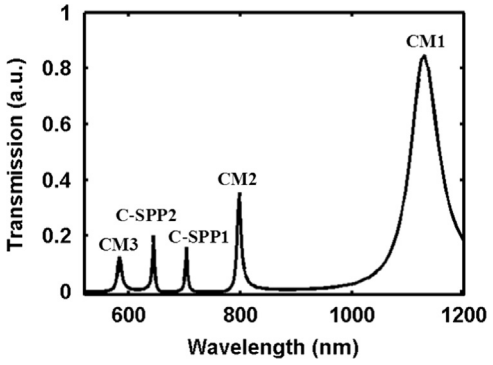

Fig. 5. Transmitted spectra of nanoslit arrays in the water (P=500 nm, W=26 nm, D=460 nm).

respectively. The largest observed shift is 2.4 nm for the peak of C-SPP2 that is associated with the top interface. When the biomolecular film is adsorbed at the top surface, the top interface will be changed from water/metal to molecules/metal, which will affect the generated SPP directly at the interface because of the changed refractive index. In general, the high sensitivity to the changes of the surrounding medium is originating from the sufficient field interaction with the targets. Contrarily, C-SPP1 and CMs just suffer a relative slight red shift because the biomolecular film don't contact with the corresponding resonance regions (C-SPP1 and CMs) directly. The different responses to the biomolecular film for the five resonance modes, suggest that our designed structure have a spectral-dependent sensing characteristics. In an ideal point-of-care testing plasmonic sensor, the transmission intensity difference spectrum ($\Delta T = (T_{ni}-T_{nj})/T0$) can be used to describe the sensing efficiency of the sensor, where the T0 is 1 for the total intensity of the light source.

In order to more accurately describe the index (ΔT), the other different refractive index of n=1.592 is used to compare and evaluate the sensing performance. As shown in Fig. 7(c), the C-SPP2 has a more remarkably narrowband spectral fluctuation and a bigger intensity difference ($\Delta T = T_{n1.592} - T_{n1.570}$) than the other modes, which could extremely enhance the spectral intensity detection and lead to high signal-to-noise ratio. Furthermore, for the case of the film adsorbing inside of the nanoslit (at the slit walls) (Fig. 7(b)), obvious wavelength red shift for CM1, CM2, CM3, C-SPP1 and C-SPP2 are 57 nm, 30.8 nm, 23.1 nm, 9.9 nm, 9.9 nm (Fig. 7(d)), respectively. The obtained red shift values show great improvements than the previous reports using gold nanoslit arrays [10]. The relatively larger wavelength red-shift for CMs can be attributed to the strongly enhanced optical field inside the nanoslits due to cavity mode resonances. Especially for the resonance CM1 and CM2, the wavelength shifts are near 24 times and 13 times of the biggest value for the case of the film adsorbing at the top surface. Significantly, as shown in Fig. 7(d), the corresponding transmission intensity difference for the case of the molecular film inside of the nanoslit is about 10 times of that of the film adsorbing at top surface (as depicted in Fig. 7(c)), which suggest that the in-slit sensing has a higher performance than that at the top metal surface. Therefore, for our designed sensor, the sensing performances are associated with the concrete positions of the adsorbing biomolecular materials, which demonstrate that it has superior performances of the spatial selective sensing and is significative for the real applications with high selectivity and purposiveness.

From the above discussions, the nanoslit arrays have a spatial and spectral selective characteristic in refractive index sensing. The simply designed structure shows a superior sensing performance when the biomolecules adsorbing inside of the slit, and the in-slit sensing has an immense potential for biomolecular sensing applications. So we further investigate the in-slit sensing characteristics by adsorbing a 1.3 nm BSA protein monolayer film with the refractive index of n=1.570 at slit walls [28]. And the target molecules adhering inside the nanoslits can be achieved in experiments very easily by coating the top metal surface with dielectric block layer and only exposing the inside metal walls of the nanoslits for molecular bindings [29]. As shown in Fig. 8(a), the obvious red shifts of 12 nm and 7 nm can be observed for the CM1, CM2 respectively. And we can also find that the CM2 has the bigger intensity difference ($\Delta T = T_{n1.570}-T_{n1.33}$) and bigger slope compared with those of CM1. In other words, the CM2 will lead to a higher signal-to-noise ratio in the spectral intensity detection. Therefore, for different adsorbing biomolecules (with different optical constants), there will be different resonance modes as the best detecting mode for the concrete cases.

The in-slit sensing characteristics could be further enhanced by properly choosing the geometric parameters, especially for the width of slits because it has an direct influence on the propagation constant of cavity mode [30]. Fig. 8(b) demonstrate the peak wavelength shifts as a function of metal nanolits' widths. Evidently, the narrower slit (smaller width) is, the larger shift (red-shift) will be obtained. For example, when we set W=10 nm, the peak shift of 35 nm can be obtained accordingly, which is around 20 times larger than that of the previous EOT-based plasmonics biosensor in near-infrared region [31]. When the width is set as 5 nm, the corresponding red-shift can reach to 80 nm nearly. That is to say that we can modulate the corresponding sensing performances of the designed plasmonics sensor by tuning the relative parameters. These results suggest that the designed nanoslit arrays have a high-performance sensing capability for biomolecular film detection with superior spatial and spectral selectivity.

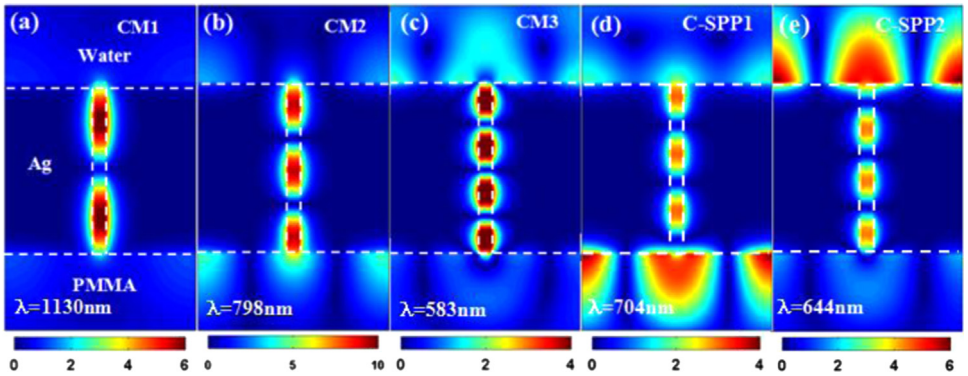

Fig. 6. Calculate magnetic field distributions at the corresponding resonance peaks of CM1, CM2, CM3, C-SPP1 and C-SPP2.

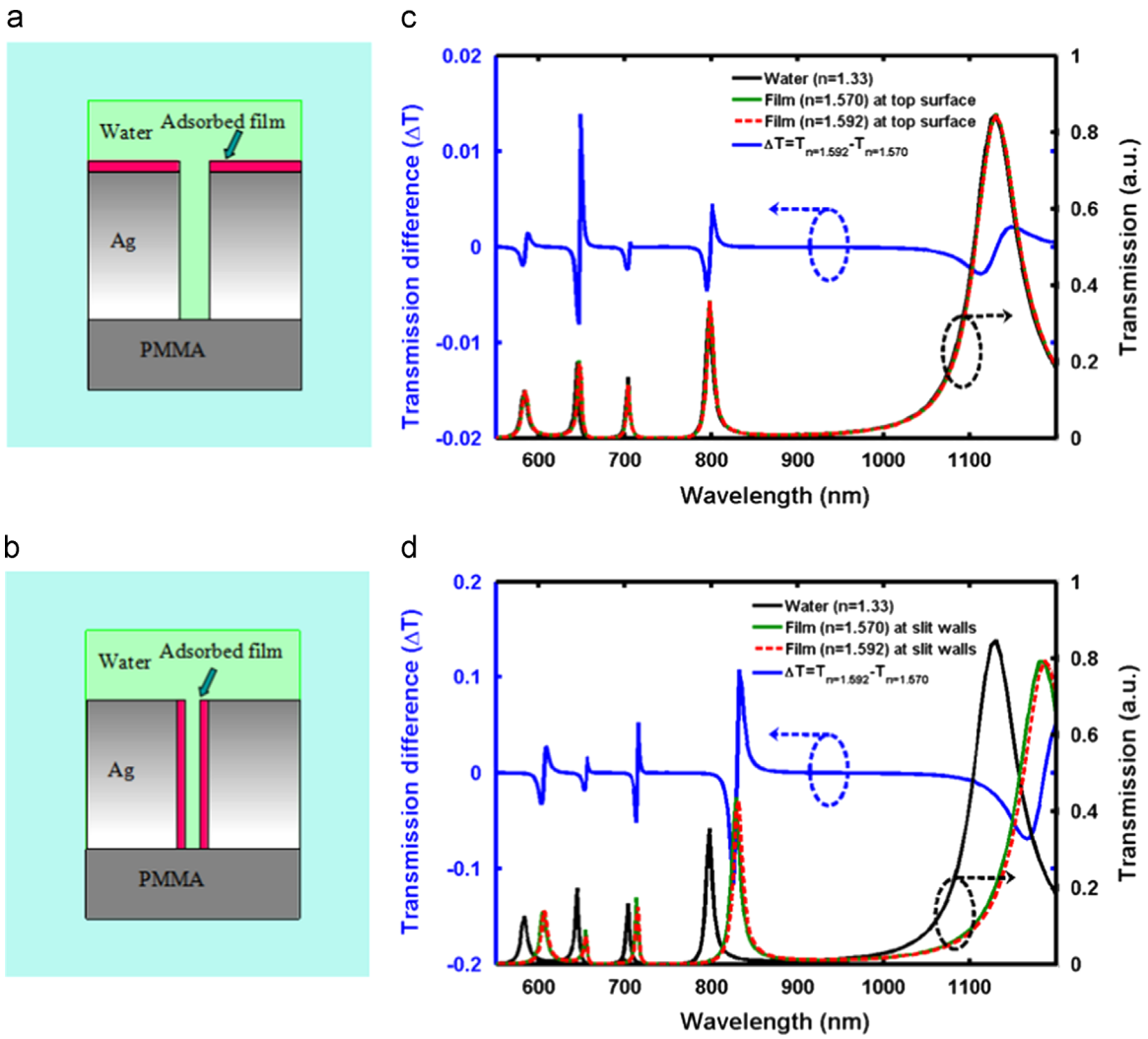

Fig. 7. Illustration of film adsorbing at the top metal surface (a) or at nanoslit walls (b). The sensor's performances of the transmission spectra and the transmission differences for the film adsorbed at the top metal surface (c) or at nanoslit walls (d).

4. Conclusion

In summary, we have systematically investigated a spatial and spectral selective plasmonic sensing based on a metallic nanoslit arrays. The structure is easy to fabricate and the SPP and CMs can coexist in the designed structure by modulating the parameters properly. By combining of the SPP, CMs and their near-field coupling effects, a multi-band spectra with different characteristics can be achieved. We have also investigated the sensor response upon molecular adsorping at different positions of nanoslit arrays. The simulated results show a superior performance of spatial and spectral selective sensing due to plasmonics confinement and near-field coupling effects at specific position, where different types of resonances occur. In addition, the simulation

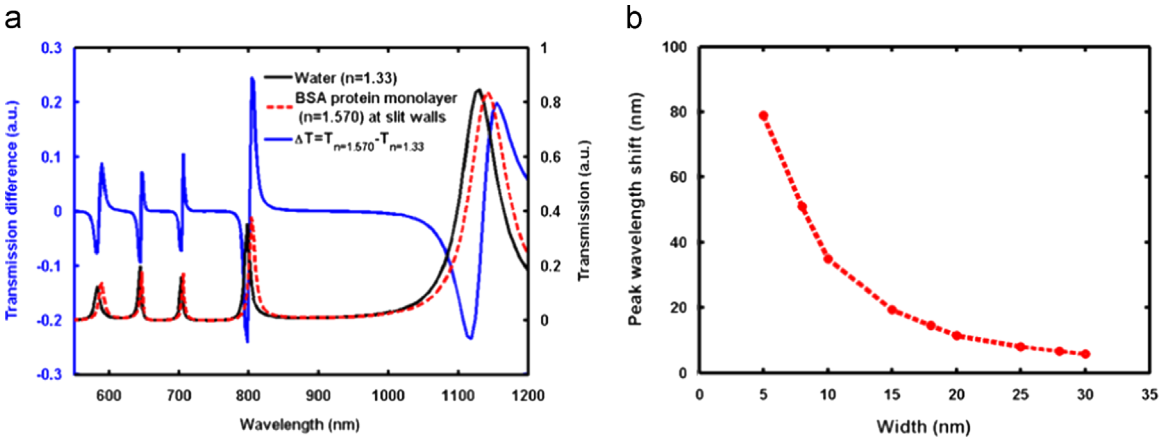

Fig. 8. Transmitted spectra and transmission difference of BSA monolayer film adhered at the nanoslit walls (a). (b) Transmission peak as a function of slit widths.

results show that the performances of the sensor can be further improved by tuning the width of nanoslits. These findings provide a basic designing guideline to optimize nanoslit arrays based sensor, and these novel features show great potential applications in the biosensing and detections.

Acknowledgements

The authors gratefully acknowledge the financial supports for this work from the Fundamental Research Funds for the Central Universities (2015HGCH0010), and the National Natural Science Foundation of China under Grant No. 61575060.

References

[1] K.A. Willets, R.P. Van Duyne, Localized surface plasmon spectroscopy and sensing, Annu. Rev. Phys. Chem. 58 (2007) 267–297.
[2] Q. Fu, D.G. Yi, M.F. Zhang, X.X. Wang, Y.K. Chen, P. Wang, H. Ming, Effect of shell thickness on a Au–Ag core–shell nanorods-based plasmonic nano-sensor, J. Opt.-UK. 14 (2012) 085001.
[3] Y. Tao, Z. Guo, A. Zhang, J. Zhang, B. Wang, S. Qu, Gold nanoshells with gain-assisted silica core for ultra-sensitive bio-molecular sensors, Opt. Commun. 349 (2015) 193–197.
[4] A.G. Brolo, Plasmonics for future biosensors, Nat. Photonics 6 (2012) 709–713.
[5] J. Homola, Surface plasmon resonance sensors for detection of chemical and biological species, Chem. Rev. 108 (2008) 462–493.
[6] P.R.H. Stark, A.E. Halleck, D.N. Larson, Short order nanohole arrays in metals for highly sensitive probing of local indices of refraction as the basis for a highly multiplexed biosensor technology, Methods 37 (2005) 37–47.
[7] A. De Leebeeck, L.S. Kumar, V. de Lange, D. Sinton, R. Gordon, A.G. Brolo, On-chip surface-based detection with nanohole arrays, Anal. Chem. 79 (2007) 4094–4100.
[8] J.W. Menezes, J. Ferreira, M.J. Santos, L. Cescato, A.G. Brolo, Large-Area fabrication of periodic arrays of nanoholes in metal films and their application in biosensing and plasmonic-Enhancedphotovoltaics, Adv. Funct. Mater. 20 (2010) 3918–3924.
[9] K.L. Lee, P.W. Chen, S.H. Wu, J.B. Huang, S.Y. Yang, P.K. Wei, Enhancing surface plasmon detection using template-stripped gold nanoslit arrays on plastic films, Acs Nano 6 (2012) 2931–2939.
[10] Y. Gao, Q. Gan, F.J. Bartoli, Spatially selective plasmonic sensing using metallic nanoslit arrays, IEEE J. Sel. Top. Quantum 20 (2014) 96–101.
[11] S. Roh, T. Chung, B. Lee, Overview of the characteristics of micro-and nano-structured surface plasmon resonance sensors, Sensors 11 (2011) 1565–1588.
[12] Z. Ruan, M. Qiu, Enhanced transmission through periodic arrays of sub-wavelength holes: the role of localized waveguide resonances, Phys. Rev. Lett. 96 (2006) 233901.
[13] S.G. Rodrigo, O. Mahboub, A. Degiron, C. Genet, F.J. García-Vidal, L. Martín-Moreno, T.W. Ebbesen, Holes with very acute angles: a new paradigm of extraordinary optical transmission through strongly localized modes, Opt. Express 18 (2010) 23691–23697.
[14] Y. Ding, J. Yoon, J.M. Haved, S.H. Song, R. Magnusson, Mapping surface-plasmon polaritons and cavity modes in extraordinary optical transmission, IEEE Photonics L 3 (2011) 365–374.
[15] R. Li, Z. Guo, W. Wang, J. Zhang, A. Zhang, J. Liu, J. Gao, Ultra-thin circular polarization analyzer based on the metal rectangular split-ring resonators, Opt. Express 22 (2014))27968–27975.
[16] J. Zhang, Z. Guo, R. Li, W. Wang, A. Zhang, J. Liu, S. Qu, J. Gao, Circular polarization analyzer based on the combined coaxial Archimedes′ spiral structure, Plasmonics (2015), http://dx.doi.org/10.1007/s11468-015-9917-2 (posted 24 Mar. 2015, in press).
[17] W. Wang, Z. Guo, R. Li, J. Zhang, Y. Li, Y. Liu, S. Qu, Plasmonics metalens independent from the incident polarizations, Opt. Express 23 (2015) 16782–16791.
[18] V.R. Machavaram, R. ABadcock, G.F. Fernando, F2-laser ablation of Fabry–Perot cavities in optical fibres: chemical sensors, J. Opt.-UK 14 (2012) 035602.
[19] P.T. Kristensen, C. Van Vlack, S. Hughes, Generalized effective mode volume for leaky optical cavities, Opt. Lett. 37 (2012) 1649–1651.
[20] X. Zhang, Z. Li, S. Ye, S. Wu, J. Zhang, L. Cui, B. Yang, Elevated Ag nanohole arrays for high performance plasmonic sensors based on extraordinary optical transmission, J. Mater. Chem. 22 (2012) 8903–8910.
[21] Z. Jakšic, D. Vasiljevic-Radovic, M. Sarajlic, Analyte-targeted patterning of subwavelength aperture arrays with extraordinary optical transmission for enhanced biosensing, in: Proceedings of the 8th International Conference on Fundamental and Applied Aspects of Physical Chemistry, Belgrade, 2006, pp. 528–530.
[22] K.L. Lee, J.B. Huang, J.W. Chang, S.H. Wu, P.K. Wei, Ultrasensitive Biosensors Using Enhanced Fano Resonances in Capped Gold Nanoslit Arrays, Sci. Rep.-UK. 5 (2015) 8547.
[23] C. Yu, J. Irudayaraj, Multiplex biosensor using gold nanorods, Anal. Chem. 79 (2007) 572–579.
[24] Z. Liu, G. Liu, S. Huang, X. Liu, P. Pan, Y. Wang, G. Gu, Multispectral spatial and frequency selective sensing with ultra-compact cross-shaped antenna plasmonic crystals, Sens. Actuators B-Chem. 215 (2015) 480–488.
[25] E.F. Schubert, Refractive index and extinction coefficient of materials, 2004. ⟨http://homepages.rpi.edu/~schubert/Educational-resources/Materials-Refractive-index-and-extinction-coefficient.pdf⟩.
[26] J.W. Yoon, M.J. Jung, S.H. Song, R. Magnusson, Analytic theory of the resonance properties of metallic nanoslit arrays, IEEE J. Quantum Elect. 48 (2012) 852–861.
[27] S.H. Chang, S. Gray, G. Schatz, Surface plasmon generation and light transmission by isolated nanoholes and arrays of nanoholes in thin metal films, Opt. Express 13 (2005) 3150–3165.
[28] L.S. Jung, C.T. Campbell, T.M. Chinowsky, M.N. Mar, S.S. Yee, Quantitative interpretation of the response of surface plasmon resonance sensors to adsorbed films, Langmuir 14 (1998) 5636–5648.
[29] J. Ferreira, M.J. Santos, M.M. Rahman, A.G. Brolo, R. Gordon, D. Sinton, E. M. Girotto, Attomolar protein detection using in-hole surface plasmon resonance, J. Am. Chem. Soc. 131 (2008) 436–437.
[30] J.A. Dionne, L. ASweatlock, H.A. Atwater, A. Polman, Plasmon slot waveguides: towards chip-scale propagation with subwavelength-scale localization, Phys. Rev. B. 73 (2006) 035407.
[31] G.M. Hwang, L. Pang, E.H. Mullen, Y. Fainman, Plasmonic sensing of biological analytes through nanoholes, IEEE Sens J. 8 (2008) 2074–2079.